ORBIT AND STELLAR PROPERTIES OF THE YOUNG TRIPLE V807 Tau

G. H. SCHAEFER[1], L. PRATO[2], M. SIMON[3], AND R. T. ZAVALA[4]

[1] The CHARA Array of Georgia State University, Mount Wilson Observatory, Mount Wilson, CA 91023, USA; schaefer@chara-array.org
[2] Lowell Observatory, 1400 West Mars Hill Road, Flagstaff, AZ 86001, USA
[3] Department of Physics and Astronomy, Stony Brook University, Stony Brook, NY 11794, USA
[4] United State Naval Observatory, Flagstaff Station, 10391 W. Naval Observatory Road, Flagstaff, AZ 86001, USA

ABSTRACT

We present new orbital measurements of the pre-main-sequence triple system, V807 Tau, using adaptive optics imaging at the Keck Observatory. We computed an orbit for the close pair, V807 Tau Ba−Bb, with a period of 12.312 ± 0.058 years and a semi-major axis of 38.59 ± 0.16 mas. By modeling the center of mass motion of the components in the close pair relative to the wide component, V807 Tau A, we measured a mass ratio of 0.843 ± 0.050 for Bb/Ba. Combined with the total mass from the relative orbit, we derived individual masses of $M_{\mathrm{Ba}} = 0.564 \pm 0.018 \, (d/140 \, \mathrm{pc})^3 \, M_\odot$ and $M_{\mathrm{Bb}} = 0.476 \pm 0.017 \, (d/140 \, \mathrm{pc})^3 \, M_\odot$ at an average distance of 140 pc to the Taurus star-forming region. We computed spectral energy distributions to determine the luminosities of the three components. We also measured their spectral types, effective temperatures, and rotational velocities based on spatially resolved spectra obtained at the Keck Observatory. If the rotational axes are aligned, then the projected rotational velocities imply that V807 Tau Ba and Bb are rotating much faster than V807 Tau A. The uncertainty in the stellar effective temperatures and distance to the system currently limit the comparison of our dynamical mass measurements with predictions based on evolutionary tracks for pre-main-sequence stars. We also report preliminary results from a program to map the 3.6 cm radio emission from V807 Tau using the Very Long Baseline Array. With continued monitoring, these observations will provide a precise parallax for placing the dynamical masses on an absolute scale.

Key words: binaries: visual – stars: fundamental parameters – stars: individual (V807 Tau) – stars: pre-main sequence

Online-only material: color figures

1. INTRODUCTION

V807 Tau (Elias 12, HBC 404) is a pre-main-sequence (PMS) hierarchical triple system located in the Taurus star-forming region. The system was resolved into two wide components at a separation of ∼300 mas by Ghez et al. (1993, 1995), Leinert et al. (1993), and Simon et al. (1996). White & Ghez (2001) and Hartigan & Kenyon (2003) identified the primary (V807 Tau A, Elias 12 S) as a K5−K7 classical T Tauri star showing signs of an accretion disk, while the secondary (V807 Tau B, Elias 12 N) was identified as an M2−M3 weak-lined T Tauri star with no evidence for accretion. Simon et al. (1995) resolved the secondary into two close components (V807 Tau Ba−Bb, Elias 12 Na−Nb) during a lunar occultation. This close pair is separated by ∼40 mas. We have been mapping the orbital motion of V807 Tau as a triple system beginning in 1999 using the Fine Guidance Sensors (FGSs) on board the *Hubble Space Telescope* and later with adaptive optics (AO) imaging at the Keck Observatory (Schaefer et al. 2003, 2006).

Mapping the orbital motion of a binary star provides a fundamental way to measure the dynamical masses of the component stars. This can be accomplished by observing eclipsing double-lined spectroscopic binaries where the radial velocity variations and timing of the eclipse light curve yield the masses and radii of the component stars (e.g., Andersen 1991). Alternatively, spatially resolving the visual orbit of a double-lined spectroscopic binary (SB2) yields the component stellar masses and distance to the system. At the distances to the nearest star-forming regions (140 pc for the Taurus star-forming region; Kenyon et al. 1994), resolving short-period PMS SB2s becomes challenging and requires high angular resolution techniques

(e.g., Steffen et al. 2001; Boden et al. 2005, 2007; Schaefer et al. 2008). With an orbital period of ∼12 years (Section 3.1), the velocity separation of the close binary components in V807 Tau is no more than a few km s^{-1}. Attempts to measure the radial velocity variations are further complicated because the spectra of V807 Tau Ba−Bb are rotationally broadened to velocity widths of 60–70 km s^{-1} (Section 2.2).

Fortunately, the triple nature of V807 Tau provides an additional technique for determining the masses of the components in the close pair. When combined with an estimate for the distance to the system, the relative visual orbit between V807 Tau Ba−Bb provides a measurement of their total mass. Additionally, the wide primary V807 Tau A provides a reference position to measure the astrometric motion of V807 Tau Ba−Bb around their center of mass, providing a direct measurement of the mass ratio between the close components. Together, these measurements give the individual masses of the components in V807 Tau Ba−Bb. A similar approach was followed to determine the masses for the components in the close pair in the T Tau triple system (Duchêne et al. 2006).

In this paper we present the results of a multi-wavelength campaign to study the V807 Tau triple system. We used infrared AO imaging at the Keck Observatory to map the astrometric motion of the close pair and present the orbital solution and component masses in Section 3.1. We also obtained spectra of the three components on several epochs using a high spectral resolution spectrometer operating with the AO system at the Keck Observatory to separate out the contribution of each component. Although we could not measure radial velocities precisely enough to determine a spectroscopic orbit, we discuss the spectral types and rotational properties of the stars within the

Report Documentation Page

1. REPORT DATE **10 SEP 2012**	2. REPORT TYPE	3. DATES COVERED **00-00-2012 to 00-00-2012**

4. TITLE AND SUBTITLE	5a. CONTRACT NUMBER
Orbit And Stellar Properties Of The Young Triple V807 Tau	5b. GRANT NUMBER
	5c. PROGRAM ELEMENT NUMBER
6. AUTHOR(S)	5d. PROJECT NUMBER
	5e. TASK NUMBER
	5f. WORK UNIT NUMBER

7. PERFORMING ORGANIZATION NAME(S) AND ADDRESS(ES) **United State Naval Observatory,Flagstaff Station,10391 W. Naval Observatory Road,Flagstaff,AZ,86001**	8. PERFORMING ORGANIZATION REPORT NUMBER

9. SPONSORING/MONITORING AGENCY NAME(S) AND ADDRESS(ES)	10. SPONSOR/MONITOR'S ACRONYM(S)
	11. SPONSOR/MONITOR'S REPORT NUMBER(S)

12. DISTRIBUTION/AVAILABILITY STATEMENT
Approved for public release; distribution unlimited

13. SUPPLEMENTARY NOTES
The Astrophysical Journal, 756:120 (14pp), 2012 September 10

14. ABSTRACT

We present new orbital measurements of the pre-main-sequence triple system, V807 Tau, using adaptive optics imaging at the Keck Observatory. We computed an orbit for the close pair, V807 Tau Ba−Bb, with a period of 12.312 ? 0.058 years and a semi-major axis of 38.59 ? 0.16 mas. By modeling the center of mass motion of the components in the close pair relative to the wide component, V807 Tau A, we measured a mass ratio of 0.843 ? 0.050 for Bb/Ba. Combined with the total mass from the relative orbit, we derived individual masses of $M_{Ba} = 0.564 ? 0.018$ (d/140 pc)3M andM$_{Bb} = 0.476 ? 0.017$ (d/140 pc)3M at an average distance of 140 pc to the Taurus star-forming region. We computed spectral energy distributions to determine the luminosities of the three components.We also measured their spectral types, effective temperatures, and rotational velocities based on spatially resolved spectra obtained at the Keck Observatory. If the rotational axes are aligned, then the projected rotational velocities imply that V807 Tau Ba and Bb are rotating much faster than V807 Tau A. The uncertainty in the stellar effective temperatures and distance to the system currently limit the comparison of our dynamical mass measurements with predictions based on evolutionary tracks for pre-main-sequence stars. We also report preliminary results from a program to map the 3.6 cm radio emission from V807 Tau using the Very Long Baseline Array. With continued monitoring, these observations will provide a precise parallax for placing the dynamical masses on an absolute scale.

15. SUBJECT TERMS

16. SECURITY CLASSIFICATION OF:			17. LIMITATION OF ABSTRACT	18. NUMBER OF PAGES	19a. NAME OF RESPONSIBLE PERSON
a. REPORT **unclassified**	b. ABSTRACT **unclassified**	c. THIS PAGE **unclassified**	**Same as Report (SAR)**	**15**	

Table 1
Log of Recent NIRC2 Adaptive Optics Observations[a]

Date	Filter	AO Rate (Hz)	T_{int} (s)	No. Co-add	No. Im.
2006 Dec 18	Jcont	492	1.00	10	10
	Hcont	492	0.60	10	10
	Kcont	492	0.50	10	10
2008 Jan 17	Hcont	438	0.40	10	20
	Kcont	438	0.40	10	20
	L'	438	0.05	10	10
2008 Dec 17	Hcont	438	0.30	10	10
	Kcont	438	0.30	10	10
2009 Oct 25	Hcont	438	0.18	10	12
	Kcont	438	0.18	10	12
2011 Jan 24	Hcont	438	0.50	10	12
	Kcont	438	0.50	10	12
2011 Oct 12	Hcont	438	0.18	10	24
	Kcont	438	0.18	10	6
	Kcont	438	0.30	10	12

Note. [a] See Schaefer et al. (2006) for a log of observations obtained prior to 2006.

system in Sections 2.2 and 4.2. Using estimates of the effective temperature and luminosity computed by fitting the spectral energy distribution (SED) for each component, we compare our dynamical measurements with predicted masses and ages from PMS evolutionary tracks in Section 4.1. We also report on the detection of 3.6 cm radio emission measured with the Very Long Baseline Array (VLBA) in Sections 2.3 and 3.3. The location of the radio emission is consistent with the infrared locations of the components in the close pair. With continued observations, the radio measurements could provide an independent measurement of the parallax of V807 Tau.

2. OBSERVATIONS AND DATA REDUCTION

2.1. Adaptive Optics Imaging

We obtained AO images of V807 Tau using the near-infrared camera NIRC2 (Wizinowich et al. 2000) on the 10 m Keck II Telescope at the W. M. Keck Observatory. The NIRC2 detector is a 1024×1024 Aladdin-3 InSb array. The images were taken with the narrow-field camera which has a plate scale of 9.952 ± 0.002 mas pixel^{-1} (Yelda et al. 2010). During each epoch, we obtained 10–20 sets of dithered images, using a three-point dither pattern with a dither offset of $\sim 2''$. The primary star V807 Tau A was used as the AO guide star.

Table 1 lists the AO observations of V807 Tau taken since Schaefer et al. (2006). The table lists the filters, AO correction rates, exposure time, number of co-added exposures per image, and total number of images obtained. The images were flat-fielded using dark-subtracted, median-filtered dome flat fields obtained on the nights of observation. Pairs of dithered exposures were subtracted to remove the sky background. Figure 1 shows co-added AO images for V807 Tau from 2002 to 2011.

The wide primary V807 Tau A is sufficiently bright and close, within the isoplanatic patch, to V807 Tau B that it can be used as a simultaneous point-spread function (PSF) for measuring the separation and flux ratio of the close pair. We extracted subarrays from the images centered on the close pair, with widths of $0''.12$–$0''.16$. We used V807 Tau A as a PSF to construct models of the close pair while searching through a grid of separations and flux ratios. We used the IDL INTERPOLATE procedure to shift the PSF by sub-pixel intervals using cubic

convolution interpolation. To remove any excess light of the primary star from the extracted subarray of the close pair, we followed a least-squares approach to fit the background as a slanting plane. We determined the position and flux ratio of the companions in the close binary from where the χ^2 between the model and the data reached a minimum. After referencing the location of the close pair to V807 Tau A in the full array, we corrected the positions for geometric distortion by using the distortion solution computed by Yelda et al. (2010). We subtracted $0''.252 \pm 0''.009$ from the measured position angles to correct for the orientation of the NIRC2 camera relative to north. We determined uncertainties in the positions and flux ratios by analyzing multiple images individually and computing the standard deviation.

Table 2 lists the separation and position angle measured for V807 Tau A−Ba, A−Bb, and Ba−Bb. The position angle is measured east of north and is referenced to the date of observation. For completeness, we also include previously published positions from Schaefer et al. (2006). We have revised the uncertainties for the close pair from the previously published values because we now use the standard deviation determined directly from the relative separation and position angle of the close pair rather than propagating the uncertainties derived from the widely spaced separations of A−Ba and A−Bb. We also corrected the previously published positions for geometric distortions in the camera.

The cumulative listing of infrared flux ratios measured for the V807 Tau triple system from the AO observations is presented in Table 3 which lists the flux ratios of Ba relative to A, Bb relative to A, and Bb relative to Ba. In the lower portion of the table we list weighted mean values for the flux ratios in the J, H, K', and L' bands. We also used the photomultiplier (PMT) counts from the FGS observations (using the F583W filter) published in Schaefer et al. (2006) to estimate the V-band flux ratios. In Table 4, we convert the flux ratios to component magnitudes by using published photometry obtained for the unresolved system. The top portion of the table lists the published photometry for the total flux of V807 Tau (Kharchenko 2001; Kharchenko & Roeser 2009; Cutri et al. 2003) as well as magnitudes for the separated northern and southern components (White & Ghez 2001). In the lower portion of the table we use these total magnitudes along with the average flux ratios in Table 3 to compute the magnitude of each component. We also use the FGS magnitude conversion (Holfeltz et al. 1995; Schaefer et al. 2003) to convert directly the mean PMT counts into V-band magnitudes of the components (using $B - V \sim 1.2$; White & Ghez 2001).

2.2. High-resolution Spectroscopy

To measure radial and rotational velocities and determine spectral types, we obtained spectra with NIRSPEC, the near-infrared, cryogenic, cross-dispersed echelle spectrograph (McLean et al. 1998, 2000) on the Keck II Telescope. Observations with NIRSPEC behind the AO system (NIRSPAO) separated the light of the V807 Tau components; additional unresolved spectra were taken with NIRSPEC alone. We centered the observations at $1.555\,\mu$m and used the 2 pixel wide slit which yielded a spectral resolution $\sim 30,000$. NIRSPAO provides a pixel scale of $0''.018$ in the cross-dispersion direction, about 10.6 times finer than the $0''.190$ scale for NIRSPEC. Table 5 summarizes the NIRSPEC and NIRSPAO observations. The diffraction-limited resolution at $1.6\,\mu$m is $\sim 0''.040$. Columns 2 and 3 list the orbital phase and separation of V807 Tau Ba−Bb during the times of the NIRSPAO observations predicted from
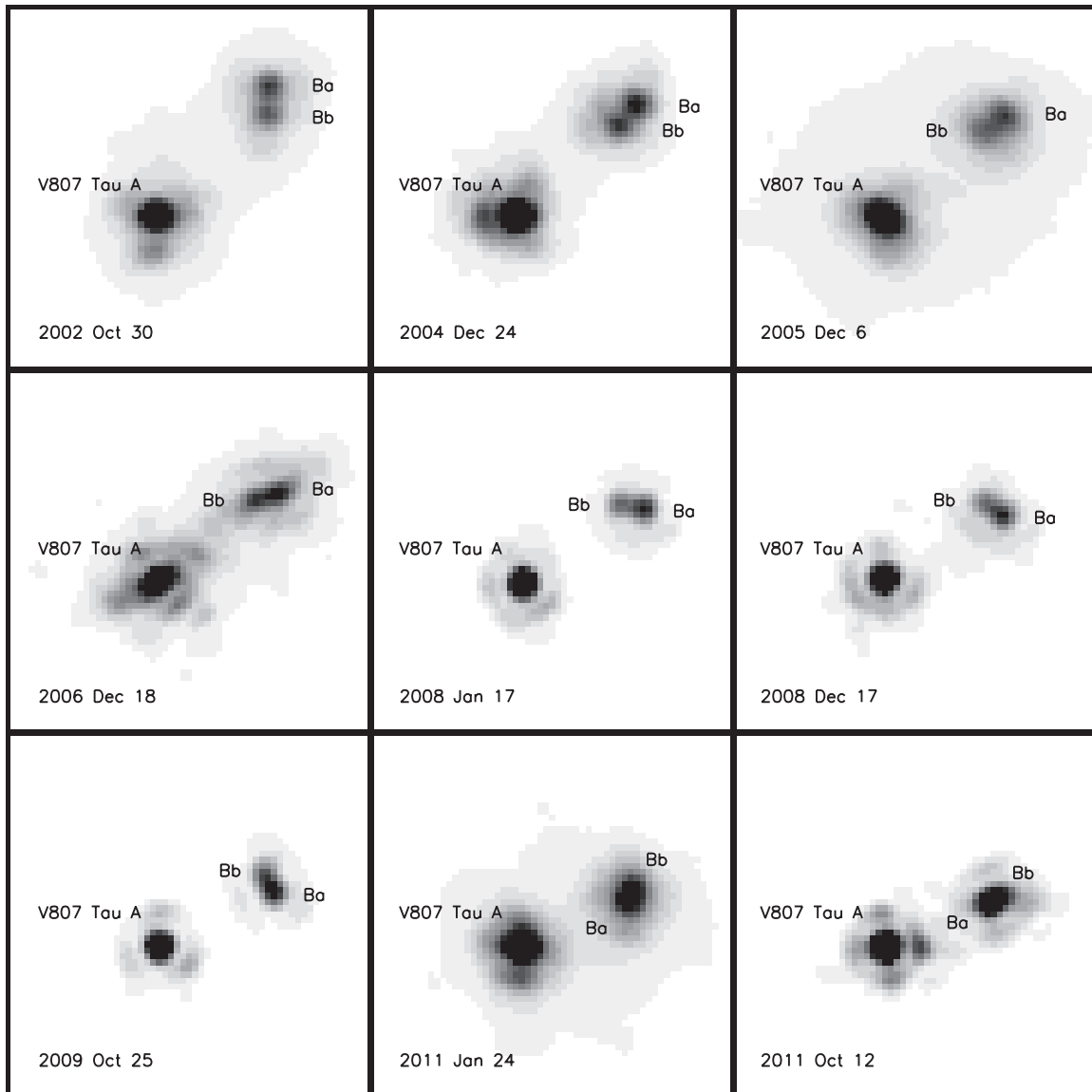
Figure 1. Keck NIRC2 adaptive optics images in the *H* band of V807 Tau obtained in 2002–2011. Each panel is 0″.6 wide, with north pointing up and east to the left. We used the wide component, V807 Tau A, as a PSF reference to model the components in the close pair. The shape of the AO-corrected PSF changes over time; this is seen most prominently in the location of the bright spots in the diffraction ring or an elongation of the core. However, for any given image, the shape of the PSF of V807 Tau A provides an excellent model of the PSFs of Ba and Bb during the same instant of time, allowing us to measure high precision positions and flux ratios of the close components.

the visual and astrometric orbital parameters (see Section 3.1). For the 2001 and 2009 AO observations, we aligned the slit along the position angle of the Ba−Bb binary; we also observed the A component separately in 2001. In 2003, 2006, and 2010, the slit was aligned along the A−B axis which was fortuitously similar to the Ba−Bb axis in 2003 and 2006. In 2010 the close binary was separated by less than 30 mas and thus unresolvable. Successful separation of the Ba−Bb components was possible only for the 2001 and 2003 data. Nodding along the slit between sequential exposures by about half the slit length enabled removal of the sky background. Exposure times ranged from 60 to 360 s; because of the reduced throughput behind the AO system, NIRSPAO spectra required longer integrations.

The spectra were reduced and extracted using the REDSPEC software package.[5] The software performs background subtraction, flat-fielding, spatial and spectral rectification, and subse-

quent extraction of the spectra. The spatial and spectral rectification removes curvature distortions in order to produce straight spectral traces. For non-AO observations the dispersion solution and wavelength calibration were computed with respect to OH night-sky lines (Rousselot et al. 2000). As a result of the reimaged optics and reduced throughput in the AO mode, the OH night-sky lines in NIRSPAO spectra are too faint to be used for wavelength calibration and the internal Ne, Ar, Xe, and Kr arc lamps were used instead. For the purpose of measuring radial velocities, only the spectra in order 49 were extracted and used in the subsequent analysis. In addition to atomic lines, this spectral region (Figure 2) contains molecular lines, most notably OH and H_2O, suitable for characterizing M and late-K spectral types, and is free of terrestrial absorption features (Prato 1998; Prato et al. 2002; Mazeh et al. 2002).

On most NIRSPAO runs, resolved spectra of V807 Tau A and B were obtained; however, V807 Tau Ba and Bb were always blended because their separations were close to or below the

---

5 http://www2.keck.hawaii.edu/inst/nirspec/redspec.html

Table 2
Relative Positions of V807 Tau from AO Imaging

Year	ρ (mas)	P.A. (°)	Ref.
V807 Tau A−Ba			
1999.7558	282.91 ± 2.10	324.31 ± 0.43	1
2000.6565	286.86 ± 1.80	323.56 ± 0.36	1
2000.6786	284.88 ± 2.70	323.60 ± 0.54	1
2001.0006	287.00 ± 1.80	322.83 ± 0.36	1
2001.1721	286.23 ± 0.91	322.12 ± 0.18	1
2002.1829	285.57 ± 0.61	320.34 ± 0.12	1
2002.8293	282.71 ± 0.34	318.90 ± 0.07	1
2002.9750	281.40 ± 1.50	319.25 ± 0.31	1
2002.9852	281.82 ± 1.10	319.60 ± 0.22	1
2003.8539	271.57 ± 1.01	317.33 ± 0.21	1
2003.9766	273.21 ± 1.00	316.96 ± 0.21	1
2005.1644	268.90 ± 1.00	312.69 ± 0.22	1
2005.5989	260.51 ± 0.70	310.92 ± 0.15	1
2005.9317	259.77 ± 0.31	309.30 ± 0.07	1
2006.9633	248.55 ± 0.47	305.51 ± 0.11	2
2008.0447	234.61 ± 0.28	301.43 ± 0.07	2
2008.9621	221.22 ± 0.25	298.08 ± 0.07	2
2009.8167	208.08 ± 0.45	295.23 ± 0.12	2
2011.0644	190.50 ± 0.39	292.97 ± 0.12	2
2011.7797	183.43 ± 0.77	292.59 ± 0.24	2
V807 Tau A−Bb			
1999.7558	305.00 ± 4.40	321.29 ± 0.83	1
2000.6565	284.59 ± 4.10	316.81 ± 0.83	1
2000.6786	285.22 ± 4.60	317.56 ± 0.92	1
2001.0006	282.86 ± 4.20	315.60 ± 0.85	1
2001.1721	279.36 ± 3.60	314.66 ± 0.74	1
2002.1829	259.74 ± 0.93	313.81 ± 0.20	1
2002.8293	249.13 ± 0.51	312.57 ± 0.12	1
2002.9750	247.05 ± 2.20	312.80 ± 0.51	1
2002.9852	248.86 ± 2.40	313.14 ± 0.55	1
2003.8539	227.53 ± 2.40	312.98 ± 0.60	1
2003.9766	228.83 ± 2.40	313.58 ± 0.60	1
2005.1644	220.81 ± 1.26	311.63 ± 0.33	1
2005.5989	214.79 ± 1.30	311.32 ± 0.35	1
2005.9317	215.27 ± 0.46	310.55 ± 0.12	1
2006.9633	209.75 ± 0.65	309.69 ± 0.18	2
2008.0447	207.72 ± 0.37	308.48 ± 0.10	2
2008.9621	208.03 ± 0.31	306.87 ± 0.08	2
2009.8167	209.40 ± 0.72	304.15 ± 0.20	2
2011.0644	210.75 ± 0.81	298.07 ± 0.22	2
2011.7797	208.02 ± 1.13	293.02 ± 0.31	2
V807 Tau Ba−Bb			
1999.7558	26.97 ± 4.88	287.78 ± 10.37	1
2000.6565	33.72 ± 4.48	226.32 ± 7.61	1
2000.6786	30.01 ± 5.33	231.24 ± 10.18	1
2001.0006	36.16 ± 4.57	222.65 ± 7.24	1
2001.1721	37.42 ± 3.71	217.83 ± 5.68	1
2002.1829	40.38 ± 1.36	187.39 ± 1.93	1
2002.8293	44.55 ± 0.34	176.91 ± 0.44	1
2002.9750	45.40 ± 2.66	176.98 ± 3.36	1
2002.9852	44.46 ± 2.64	178.63 ± 3.40	1
2003.8539	47.90 ± 2.60	158.42 ± 3.11	1
2003.9766	46.78 ± 2.60	153.75 ± 3.18	1
2004.9814	47.80 ± 1.72	138.71 ± 2.06	1
2005.1644	48.28 ± 1.46	137.54 ± 1.73	1
2005.5989	45.76 ± 1.48	129.03 ± 1.85	1
2005.9317	44.80 ± 0.47	123.28 ± 0.61	1
2006.9633	42.22 ± 0.49	104.29 ± 0.67	2
2008.0447	38.22 ± 0.36	79.57 ± 0.54	2
2008.9621	35.42 ± 0.41	54.28 ± 0.67	2
2009.8167	32.47 ± 0.41	27.38 ± 0.73	2
2011.0644	26.99 ± 0.51	336.96 ± 1.08	2
2011.7797	24.64 ± 0.52	296.16 ± 1.22	2

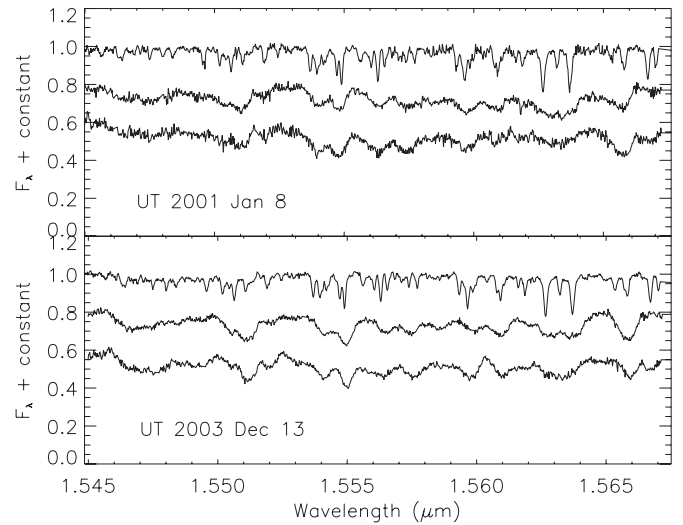**References.** (1) Schaefer et al. 2006; (2) This paper.

Figure 2. Angularly resolved spectra of V807 Tau A (top), Ba (middle), and Bb (bottom) at two epochs. The spectra are corrected for barycentric motion, normalized to 1.0, and offset by a constant.

diffraction limit. Nonetheless, when the components were at favorable separation and the AO correction particularly good, the 0″.018 pixel^{-1} scale of the detector in the cross-dispersion direction enabled us to extract individual spectra for Ba and Bb by fitting two Gaussians to the spatial profile of the data at each pixel, and thus wavelength, across order 49. We were able to extract unique spectra of Ba and Bb on 2001 January 8 and 2003 December 13 but were unable to separate the spectra from the later NIRSPAO runs when the components were at smaller separations. The unresolved spectra are designated Ba+Bb in Table 5.

We used our suite of NIRSPEC spectral templates (Prato et al. 2002; Bender et al. 2005) to identify by cross-correlation the template that best represented the spectrum of V807 Tau A and to measure its heliocentric radial velocity and rotational broadening. We determined the best fit by varying the spectral template and the applied rotational broadening to produce the highest cross-correlation coefficient; the radial velocity is given by the location of the peak. HR 8086, a K7V spectral type star, gave the best fit for V807 Tau A; the measured heliocentric radial velocities and rotational broadening are listed in Table 6. The average value and standard deviation of the radial velocity, 15.79 ± 0.65 km s^{-1}, is a good approximation to the systemic velocity of the V807 Tau triple.[6] The small downward trend in radial velocity at a rate of -0.15 ± 0.04 km s^{-1} per year is consistent with the amount of orbital motion that would be expected between the wide A–B pair. The broadening of the spectral lines indicates that V807 Tau A is rotating with a projected velocity of $\sim 15 \pm 3$ km s^{-1}.

We applied the same analysis to the angularly resolved spectra of V807 Tau Ba and Bb. We obtained the best fit to the Ba spectrum with the template of Gl 752A, an M2V spectral type star, rotationally broadened to 65–70 km s^{-1}. The result for Bb is similar; the spectra are best fit by Gl 436 (M2.5V) and Gl 752A rotationally broadened to 60–70 km s^{-1}. The difference in spectral types of the two fits is not significant because the precision of spectral type determination is no

_____
[6] At the $\sim$140 pc distance of the Taurus star-forming region the projected orbital separation of the 0″.3 V807 Tau A−B triple is about 43 AU. Assuming a circular orbit and total mass 1.5 $M_\odot$, the period is about 230 years, much greater than the orbital period of the Ba−Bb binary.

Table 3
Flux Ratios Measured for V807 Tau

Date	Filter	Ba/A	Bb/A	Bb/Ba
2002 Mar 8	H	0.388 ± 0.017	0.279 ± 0.008	0.720 ± 0.043
2002 Mar 8	K'	0.399 ± 0.011	0.276 ± 0.008	0.692 ± 0.026
2002 Oct 30	H	0.381 ± 0.016	0.266 ± 0.010	0.698 ± 0.010
2002 Oct 30	K'	0.322 ± 0.010	0.233 ± 0.008	0.723 ± 0.008
2004 Dec 24	H	0.710 ± 0.048	0.556 ± 0.031	0.784 ± 0.045
2004 Dec 24	K'	0.606 ± 0.053	0.452 ± 0.024	0.748 ± 0.043
2005 Mar 1	Hcont	0.393 ± 0.009	0.271 ± 0.008	0.689 ± 0.032
2005 Mar 1	Kcont	0.308 ± 0.012	0.224 ± 0.013	0.731 ± 0.074
2005 Dec 6	H	0.388 ± 0.003	0.284 ± 0.003	0.731 ± 0.008
2005 Dec 6	K'	0.326 ± 0.008	0.240 ± 0.007	0.736 ± 0.004
2006 Dec 18	Jcont	0.367 ± 0.010	0.277 ± 0.009	0.757 ± 0.037
2006 Dec 18	Hcont	0.363 ± 0.007	0.256 ± 0.007	0.706 ± 0.027
2006 Dec 18	Kcont	0.295 ± 0.005	0.223 ± 0.003	0.758 ± 0.019
2008 Jan 17	Hcont	0.371 ± 0.006	0.252 ± 0.004	0.678 ± 0.007
2008 Jan 17	Kcont	0.291 ± 0.003	0.212 ± 0.003	0.729 ± 0.008
2008 Jan 17	L'	0.194 ± 0.027	0.109 ± 0.024	0.593 ± 0.230
2008 Dec 17	Hcont	0.360 ± 0.005	0.243 ± 0.004	0.675 ± 0.009
2008 Dec 17	Kcont	0.282 ± 0.002	0.199 ± 0.002	0.707 ± 0.012
2009 Oct 25	Hcont	0.396 ± 0.004	0.282 ± 0.003	0.711 ± 0.009
2009 Oct 25	Kcont	0.307 ± 0.009	0.230 ± 0.008	0.749 ± 0.048
2011 Jan 24	Hcont	0.401 ± 0.006	0.265 ± 0.006	0.660 ± 0.023
2011 Jan 24	Kcont	0.342 ± 0.007	0.219 ± 0.008	0.642 ± 0.037
2011 Oct 12	Hcont	0.387 ± 0.004	0.273 ± 0.004	0.705 ± 0.011
2011 Oct 12	Kcont	0.312 ± 0.020	0.204 ± 0.022	0.660 ± 0.111
Weighted mean	V	0.1336 ± 0.0035	0.0635 ± 0.0026	0.4688 ± 0.0221
Weighted mean	J	0.3666 ± 0.0105	0.2773 ± 0.0092	0.7572 ± 0.0373
Weighted mean	H	0.3849 ± 0.0016	0.2713 ± 0.0014	0.6995 ± 0.0034
Weighted mean	K	0.2956 ± 0.0016	0.2146 ± 0.0013	0.7313 ± 0.0028
Weighted mean	L	0.194 ± 0.027	0.109 ± 0.024	0.593 ± 0.230

Table 4
Magnitudes of the Components in V807 Tau

Component	V	J	H	K	L	Ref.
V807 Tau	11.185 ± 0.114	8.146 ± 0.023	7.357 ± 0.026	6.960 ± 0.016	$\cdots$	1,2
V807 Tau A	11.56 ± 0.02	$\cdots$	$\cdots$	7.36 ± 0.05	6.54 ± 0.14	3
V807 Tau B	13.35 ± 0.04	$\cdots$	$\cdots$	8.21 ± 0.10	7.94 ± 0.14	3
V807 Tau A	11.380 ± 0.114	8.686 ± 0.025	7.905 ± 0.026	7.408 ± 0.016	$\cdots$	4
V807 Tau A	11.400 ± 0.390	$\cdots$	$\cdots$	$\cdots$	$\cdots$	5
V807 Tau Ba	13.566 ± 0.117	9.775 ± 0.034	8.941 ± 0.026	8.731 ± 0.017	$\cdots$	4
V807 Tau Ba	13.767 ± 0.043	$\cdots$	$\cdots$	8.806 ± 0.100	8.445 ± 0.220	6
V807 Tau Ba	13.572 ± 0.390	$\cdots$	$\cdots$	$\cdots$	$\cdots$	5
V807 Tau Bb	14.373 ± 0.122	10.078 ± 0.039	9.321 ± 0.026	9.078 ± 0.017	$\cdots$	4
V807 Tau Bb	14.590 ± 0.054	$\cdots$	$\cdots$	9.146 ± 0.100	9.013 ± 0.334	6
V807 Tau Bb	14.368 ± 0.392	$\cdots$	$\cdots$	$\cdots$	$\cdots$	5

References. (1) Kharchenko & Roeser 2009 (*V* band); (2) Cutri et al. 2003 (2MASS *J*, *H*, *K$_s$*); (3) White & Ghez 2001 (*V*, *K*); (4) flux ratio (A:Ba:Bb) combined with Johnson V All-sky compiled Catalog (Kharchenko & Roeser 2009) and 2MASS *J*, *H*, *K*; (5) calibrated FGS; (6) flux ratio (Ba:Bb) combined with White & Ghez (2001).

Table 5
Log of NIRSPEC/NIRSPAO Observations

UT Date	Phase	Sep (mas)	Spectra
2001 Jan 8	0.15	33	A, Ba, Bb
2002 Jul 16	0.27	43	Blended, non-AO
2002 Dec 14	0.31	45	Blended, non-AO
2003 Dec 13	0.39	47	A, Ba, Bb
2006 Dec 14	0.63	42	A, Ba+Bb
2009 Dec 6	0.88	32	Ba+Bb
2010 Dec 12	0.96	28	A, Ba+Bb

better than $\pm$ one subtype. The spectral types are consistent with the determinations of the unresolved Ba−Bb binary from broadband photometry (White & Ghez 2001) and the visible light spectrum (Hartigan & Kenyon 2003). We were unable to measure consistent radial velocities of Ba and Bb using stellar templates, or consistent velocity differences between the radial velocities of Ba and Bb by using one spectrum as the template for the other. We estimate the uncertainty of these measurements as $\geqslant \pm 5$ km s^{-1}. We were also unable to measure consistent radial velocities of the unresolved Ba + Bb spectra by two-dimensional cross-correlation with stellar templates. Figure 3 shows predicted radial velocities versus phase of Ba
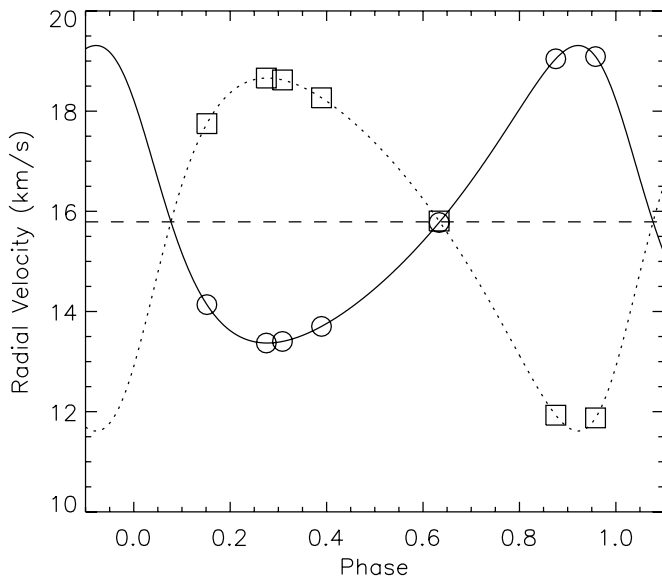
Figure 3. Predicted radial velocity curves for V807 Tau Ba (solid line) and Bb (dotted line) based on the orbital parameters and mass ratio from the visual and astrometric orbit. The circles and squares show the expected radial velocities of Ba and Bb, respectively, during the times of the NIRSPEC observations.

Figure 4. VLBA source positions of V807 Tau relative to the primary phase reference calibrator (circle) and the secondary phase reference check sources (squares).

and Bb and illustrates the difficulty in measuring their velocities. The predicted velocities were calculated using the orbital parameters and mass ratio $M_{Bb}/M_{Ba} = 0.843$ in Section 3.1, systemic velocity, and 140 pc distance to the Taurus star-forming region. The predicted velocity differences are never greater than $\sim 7.7 \, km \, s^{-1}$. It was not possible to distinguish such small differences in radial velocities of Ba and Bb given the significant broadening of their spectra.

The observed templates used for the cross-correlation analysis are main-sequence field objects while the components in V807 Tau are young stars still contracting to the main sequence. Hence, the PMS stars will have smaller surface gravities by about 0.3–0.5 in $\log g$. Metal lines are weakly dependent on $\log g$ (Blake et al. 2007; Schlieder et al. 2012); the line centers remain the same while the equivalent width of most lines decreases with increasing $\log g$. Therefore, the gravity dependence has no effect on our measurement of the radial velocities which are dominated by the location of the lines (e.g., Simon & Prato 2004; Rosero et al. 2011) and only a negligible effect on the rotational broadening for lines as broad as those of V807 Tau Ba and Bb.

2.3. VLBA Radio Interferometry

Radio emission from V807 Tau was first detected by O'Neal et al. (1990) using the Very Large Array. During two out of three epochs in 1986–1987, they measured a flux density of 0.7–1.2 mJy at 6 cm. We began a program to measure the radio emission at high resolution using the VLBA in 2007–2009. Our goals were to determine where in the system the radio emission comes from and to map the astrometric position over time to determine a parallax for the system (e.g., Lestrade et al. 1999; Loinard et al. 2005, 2008; Torres et al. 2007, 2009, 2012).

The VLBA (Napier et al. 1994; Napier 1995) consists of ten 25 m antennas spread across the United States territory from Saint Croix, VI to Mauna Kea, HI with baselines ranging from 236 to 8611 km. The signals are combined interferometrically by a correlator in Socorro, NM. We obtained six epochs of phase-referenced observations on V807 Tau at 3.6 cm (8.42 GHz) during 2007–2009. Each observation lasted a total of 10 hr, with
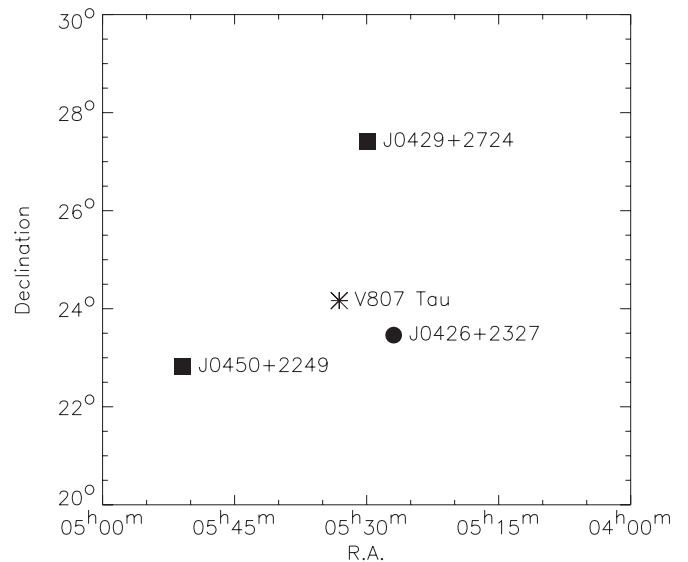
~ 4 hr spent on V807 Tau. During each observation, we observed in cycles spending 2 minutes on V807 Tau and 1 minute on the primary phase reference calibrator J0426+2327=0423+233 located 1°6 away ($F_\nu = 0.14$ Jy at 3.6 cm).[7] Every 30 minutes we observed 1 minute integrations on the phase reference check sources J0429+2724=0426+273 and J0450+2249=0447+227 located 3°3 and 4°3 away, respectively ($F_\nu = 0.32$ and 0.12 Jy). The location of these three phase sources on the sky provides good coverage around V807 Tau, as shown in Figure 4. During the first exploratory observation, we used only J0426+2327 and J0429+2724 and spent 3 minutes on source and 2 minutes on the phase reference calibrators. In all of the epochs, we observed the fringe-finder 3C 84 twice during each night. We also observed three sets of 6–7 calibration sources covering a range of elevations spaced apart in time by about 4 hr. These sources were observed using a wide bandwidth frequency setup to compute multi-band delays and correct for errors in the troposphere model.

We reduced and calibrated the VLBA data using the Astronomical Image Processing System (AIPS; van Moorsel et al. 1996) developed by NRAO following the standard procedures for reducing VLBA data. This includes applying ionospheric corrections, updating Earth orientation parameters, amplitude calibration, correction to phases for the parallactic angle of the antennas, and removal of instrumental delay residuals. We corrected for errors in the tropospheric models by using the DELZN procedure (Mioduszewski & Kogan 2009) to model the multi-band delay on the wide-band calibrator sets. We performed a global fringe fit to remove global frequency and time-dependent errors. We used the primary and secondary phase calibrators to measure and correct for the phase gradient on the sky using the ATMCA routine (Fomalont & Kogan 2005). We produced cleaned images using the difmap routine[8] (Shepherd 1997) with natural weighting (equal weighting of all data points) to provide higher sensitivity on weak sources. Reading the image back into AIPS, we used the JMFIT task to solve for the position, integrated intensity, and angular size of the source by fitting a

---

[7] http://www.vlba.nrao.edu/astro/calib/vlbaCalib.txt
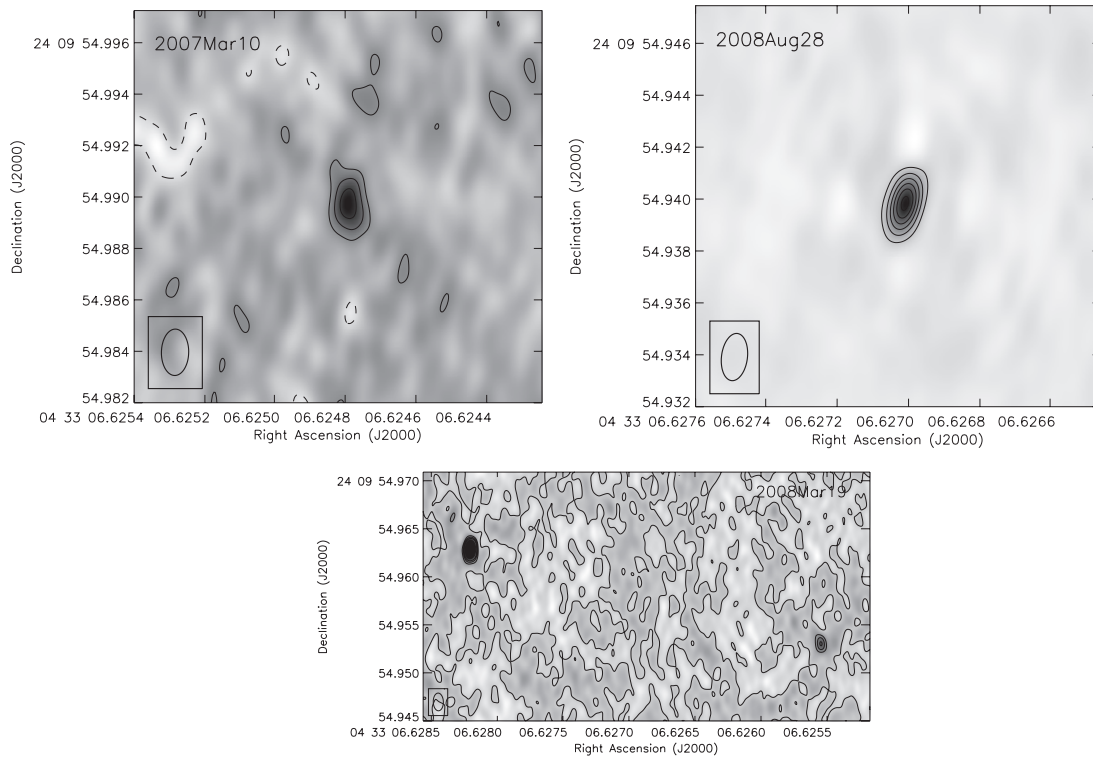[8] ftp://ftp.astro.caltech.edu/pub/difmap/difmap.html

6

Figure 5. VLBA maps of V807 Tau at 3.6 cm obtained on 2007 March 10, 2008 March 19, and 2008 August 28. The contours correspond to intervals of the uncertainty in the integrated flux given by $[-1, 1, 2, 3] \times \sigma$, $[0, 2, 3, 4, 6, 8, 10] \times \sigma$, $[5, 10, 15, 25, 30] \times \sigma$, respectively, for each epoch. The inset shows the size and orientation of the synthesized beam.

Table 6
NIRSPEC/NIRSPAO Results

UT Date	JD − 2,400,000		V807 Tau A			V807 Tau Ba		V807 Tau Bb	
		SpT	$v \sin i$ (km s^{-1})	$v_{\rm rad}$ (km s^{-1})		SpT	$v \sin i$ (km s^{-1})	SpT	$v \sin i$ (km s^{-1})
2001 Jan 8	51917.8472	K7	15	16.22 ± 1.0		M2	70 ± 10	M2	70 ± 10
2002 Jul 16	52472.1403	K7	15	16.42 ± 1.0					
2002 Dec 14	52622.8764	K7	15	16.35 ± 1.0					
2003 Dec 13	52986.8697	K7	15	15.55 ± 1.0		M2	65 ± 10	M2.5	60 ± 10
2006 Dec 14	54083.9033	K7	15	15.40 ± 1.0					
2010 Dec 12	55542.8255	K7	15	14.80 ± 1.0					
Average			15	15.79 ± 0.65			68 ± 7		65 ± 7

Table 7
VLBA Observations of V807 Tau

Date	Comp	R.A. (hh:mm:ss)	Decl. (dd:mm:ss)	f_ν (mJy)	Major (mas)	Minor (mas)	P.A. (°)
2007 Mar 10	Ba	04 33 06.6247856	24 09 54.989774	0.52 ± 0.10	2.27 ± 0.29	1.18 ± 0.15	8.3 ± 7.4
2008 Mar 19	Ba	04 33 06.6255328	24 09 54.953108	0.59 ± 0.13	2.11 ± 0.34	1.88 ± 0.30	48 ± 58
2008 Mar 19	Bb	04 33 06.6281980	24 09 54.962855	1.07 ± 0.09	1.90 ± 0.09	1.08 ± 0.05	178.5 ± 3.3
2008 Jun 4	⋯	⋯	⋯	<0.22	⋯	⋯	⋯
2008 Aug 28	Ba	04 33 06.6270069	24 09 54.939863	8.60 ± 0.27	1.86 ± 0.03	1.00 ± 0.02	164.2 ± 1.1
2008 Dec 10	⋯	⋯	⋯	<0.27	⋯	⋯	⋯
2009 Mar 6	⋯	⋯	⋯	<0.26	⋯	⋯	⋯

two-dimensional Gaussian model to the data. The results from the fit are presented in Table 7 which gives the R.A. and decl. coordinates, integrated intensity, major and minor axes (FWHM), and position angle of the Gaussian model. We detected compact radio emission in three of the six epochs of VLBA observations. On 2007 March 10 and 2008 August 28 we detected a single source and on 2008 March 19 we detected two sources.

The integrated intensity ranges between 0.52 and 8.60 mJy. The non-detections during the remaining three epochs were likely caused by intrinsic variability of the source. By imaging the phase reference and check sources during each of the VLBA epochs, we determined that our measured source coordinates are consistent with the catalog positions of the calibrators to better than 0.15 mas. Figure 5 shows the cleaned images of
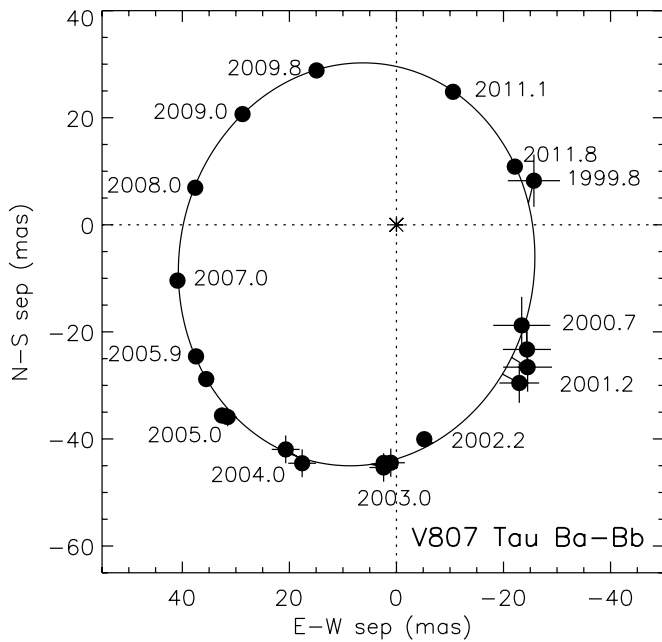
Figure 6. Orbital motion of V807 Tau Bb relative to Ba based on our adaptive optics and FGS observations. Overplotted is the best-fit orbit.

Table 8
Orbital Parameters and Masses for V807 Tau Ba−Bb

Parameter	Value
P (yr)	12.312 ± 0.058
T	1999.154 ± 0.070
e	0.2922 ± 0.0033
a (mas)	38.59 ± 0.16
i (°)	151.59 ± 0.89
Ω (°)	1.8 ± 1.6
ω (°)	50.6 ± 1.3
χ^2	15.49
χ_ν^2	0.443
$M_{\text{tot}}\,(d/140\,\text{pc})^3\,(M_\odot)$	1.040 ± 0.016
$M_{\text{Bb}}/M_{\text{Ba}}$	0.843 ± 0.050
$M_{\text{Ba}}\,(d/140\,\text{pc})^3\,(M_\odot)$	0.564 ± 0.018
$M_{\text{Bb}}\,(d/140\,\text{pc})^3\,(M_\odot)$	0.476 ± 0.017

Notes. The uncertainty in the masses represent the errors computed from the orbit fit; the systematic uncertainty in the distance is reflected by the additional scaling factor of $(d/140\,\text{pc})^3$. The uncertainty in the average distance to the Taurus star-forming region (± 10 pc; Kenyon et al. 1994) could shift the masses by as much as 0.24 $M_\odot$.

V807 Tau during the three epochs with detected emission. The position of the radio emission is consistent with the location of the components in the close pair, V807 Tau Ba and Bb (see Section 3.3 for more details).

The radio emission from V807 Tau is most likely non-thermal and thus is expected to be polarized. While the phase-referenced observations were not planned with polarimetry in mind, we performed a polarization calibration in order to learn what we could from detections or limits on the polarized flux. We solved for the right–left (R−L) phase difference (Cotton 1993) using the AIPS task RLDLY and used our weakly polarized fringe-finder 3C 84 to determine the R−L delay. We solved for the instrumental polarization (D-terms) using the AIPS task LPCAL (Leppänen et al. 1995) applied to the phase reference source J0426+2327. To examine the success of our polarization calibration we imaged 3C 84 in Stokes Q and U and made a polarized intensity image. We found the southern lobe of 3C 84 to be weakly polarized. Fortuitously, calibrated polarization images of 3C 84 were available via the publicly accessible MOJAVE archive (Lister et al. 2009). 3C 84 was observed on 2008 August 25 and the southern lobe was weakly polarized at a location coincident with our detection. Satisfied that the polarization calibration worked well enough we imaged V807 Tau in Stokes Q, U, and V using the 2008 August 28 data. This date had a sufficient Stokes I flux that even a small fractional polarization might be detected. We found no detectable polarized flux at this epoch and set 3σ limits on the fractional linear polarization of $<11\%$ and on the fractional circular polarization of $<8\%$.

3. ANALYSIS

3.1. Orbital Solution

Figure 6 shows the relative motion observed for the close pair based on the measurements listed in Table 2, where the position of V807 Tau Bb is plotted relative to V807 Tau Ba. Over 10 years of FGS and AO observations, the close pair has moved through

a complete orbit. We computed an orbit for the close pair using a standard Newton–Raphson technique. Table 8 lists the best-fitting orbital parameters for the period P, time of periastron T, eccentricity e, semi-major axis a (in mas), inclination i, position angle of the line of nodes Ω, and the longitude of periastron ω. The χ^2 and reduced χ_ν^2 of the fit are also listed in the table. The uncertainties were estimated from the diagonal elements of the covariance matrix. The orbit, with a period of 12.3 years and a semi-major axis of 38.6 mas, is overplotted in Figure 6. At an average distance to the Taurus star-forming region of 140 pc (Kenyon et al. 1994), Kepler's third law yields a total mass of $M_{\text{tot}} = 1.040 \pm 0.016\,(d/140\,\text{pc})^3\,M_\odot$.

In Schaefer et al. (2006) we presented a variety of possible orbit fits for V807 Tau Ba−Bb based on a limited number of early FGS, AO, and lunar occultation measurements (we refer to the system as "Elias 12 Na-Nb" in the previous paper). Based on the preliminary analysis of orbits that fit the available data at the time, we originally estimated that the period of V807 Tau Ba−Bb ranged from 9 to 12 years. This is quite close to the actual period of 12.312 ± 0.058 years that we measure with improved accuracy and precision because the orbital motion now covers a full orbital period. Moreover, the total mass determined from the statistical analysis of orbits that fit the data presented in Schaefer et al. (2006; $1.13^{+0.36}_{-0.09}\,M_\odot$) agrees within 1σ with our results, confirming our earlier conclusion that it is possible to derive a reasonable estimate of the total mass in a binary with limited orbital coverage because of the tight correlation between P and a. The total mass we derived in Schaefer et al. (2006) when we added the lunar occultation observation from Simon et al. (1995) to improve the time coverage of the limited set of orbital measurements ($1.026 \pm 0.068\,M_\odot$) also agrees quite well with our more precise current value. We do not include the lunar occultation within our current solution because it represents only a one-dimensional measurement of the projected separation along the direction of the occultation and we currently have sufficient orbital coverage to measure the period reliably without including it. Nonetheless, the projected separation measured in the 1992 occultation agrees within 5.3 mas (2.3σ) with the separation predicted from our orbit fit. Including the lunar occultation in the fit only marginally changes
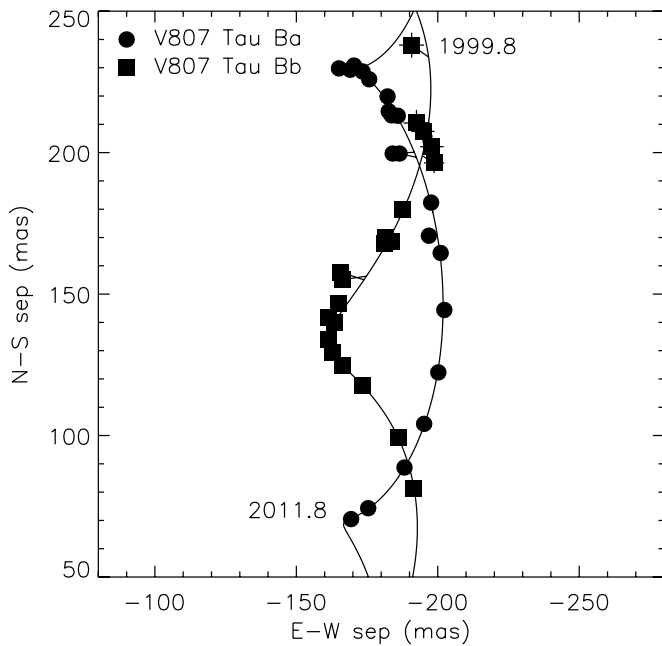
Figure 7. Astrometric motion of V807 Tau Ba (circles) and Bb (squares) relative to the wide component V807 Tau A (located at 0,0). The solid lines show the astrometric motion of the close binary components with a mass ratio of 0.843.

Figure 8. Motion of the center of mass of V807 Tau Ba−Bb (filled circles) relative to V807 Tau A, computed from the derived mass ratio of 0.843 and the measured positions of the close components relative to V807 Tau A. Overplotted is the representative orbit derived for the center of mass motion. For comparison we plot the measured positions of the wide pair V807 Tau A−B (filled squares) reported in the literature (Ghez et al. 1995; Simon et al. 1996; White & Ghez 2001; Hartigan & Kenyon 2003).

the orbital parameters within their 1σ error bars, but it also raises the χ^2 from 15.4 to 20.1 because of the 2.3σ disagreement with the measured projected separation.

The wide component, V807 Tau A, is located within ∼250 mas of the close pair and lies within the AO field of view. This allows us to map the astrometric motion of the close pair relative to V807 Tau A and model the motion of Ba and Bb around their center of mass. Figure 7 shows the motion of V807 Tau Ba and Bb as measured relative to V807 Tau A. We derived a value for the mass ratio of the close pair (M_{Bb}/M_{Ba}) by modeling the center of mass motion of V807 Tau B relative to V807 Tau A. To do this, we searched through a range of mass ratios and computed the expected location of the center of mass of V807 Tau Ba−Bb during each epoch based on the given mass ratio and the measured positions of Ba and Bb relative to V807 Tau A (Table 2). For each trial mass ratio, we then fit a representative orbit to the center of mass motion of B relative to A and selected the mass ratio that minimized the χ^2 between the calculated position of the center of mass and the orbit fit (see Figure 8). An incorrect mass ratio will produce residual reflex motion that cannot be fit by a simple Keplerian orbit.

We do not have enough coverage to determine a definitive orbit for the wide A–B pair; however, it is only necessary to find a representative orbit that adequately describes the orbital motion of the center of mass over the time frame of our measurements. In fact, there is a large range of orbits that can fit the limited data equally as well (e.g., see Figures 3, 5, and 10 in Schaefer et al. 2006, which show examples of how a family of possible orbits can fit a limited number of measurements for an incomplete orbit). To optimize the fit to the center of mass motion, we searched through a grid of possible orbits for each mass ratio explored. The possible orbits were selected by randomly choosing P, T, e over a range of values and performing a least-squares fit to optimize the remaining parameters following the method described in Schaefer et al. (2006) (see also Hartkopf et al. 1989). We searched through periods ranging from 100 to 500 years, eccentricities from 0
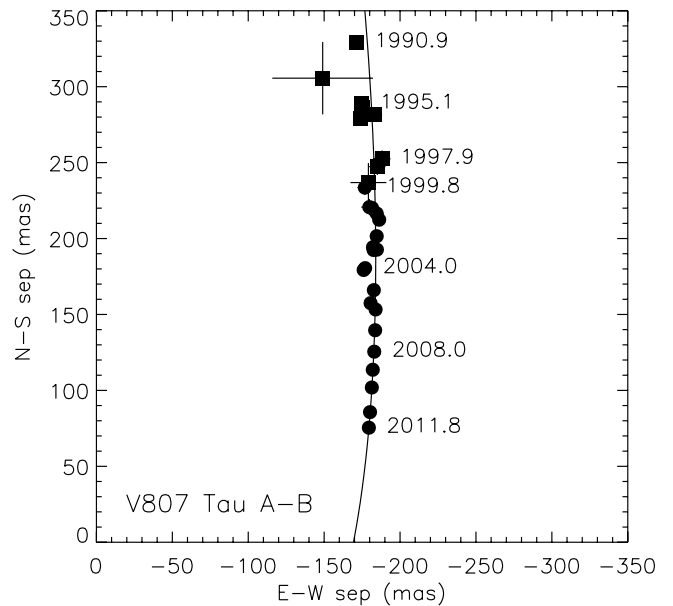
to 0.99, and allowed the time of periastron passage to vary within one orbital period. For each mass ratio, we selected the "best-fitting" representative orbit that minimized χ^2 between the calculated position of the center of mass and the orbit fit. We then selected the mass ratio that produced the smallest χ^2 as the best fit. We determined the uncertainty in the mass ratio from the 1σ confidence interval ($\Delta\chi^2 = 1$). When combined with the total mass, the best-fitting mass ratio of 0.843 ± 0.050 yields individual masses of $M_{Ba} = 0.564 \pm 0.018$ $(d/140\,\text{pc})^3$ $M_\odot$ and $M_{Bb} = 0.476 \pm 0.017$ $(d/140\,\text{pc})^3$ $M_\odot$.

The dynamical masses were computed using the average distance of 140 pc to the Taurus star-forming region (Kenyon et al. 1994) and scale as $(d/140\,\text{pc})^3$. Including the ± 10 pc uncertainty in the average distance to the masses contributes an additional systematic uncertainty of ± 0.24 $M_\odot$ to the error budget. Star formation in Taurus occurred in several clumps. Several individual members in the region are known to have precise distances ranging from 128.5 pc for Hubble 4 and 161.2 pc for HP Tau/G2 (Torres et al. 2009, and references therein). The position on the sky of V807 Tau is near HP Tau/G2; if its distance is similar too, then the actual masses will be $(160/140)^3 \sim 1.5$ times larger. VLBA observations to measure the distance to V807 Tau (see Sections 2.3 and 3.3) are in progress.

3.2. Spectral Energy Distributions

We constructed SEDs for each of the three components, V807 Tau A, Ba, and Bb, using the magnitudes listed in Table 4. We converted the observed magnitudes m_λ to measured fluxes through

$$F_{\lambda,\text{meas}} = F_{\lambda_0} \times 10.0^{-0.4[m_\lambda - A_\lambda]}, \qquad (1)$$

where A_λ is the wavelength-dependent interstellar extinction assuming an $R = 3.1$ reddening law (Cardelli et al. 1989; O'Donnell 1994) and F_{λ_0} is the zero-point flux density for

Table 9
Spectral Energy Distributions

Star	SpT	T_{eff} (K)	A_V (mag)	θ (mas)	F_{bol} (10^{-9} erg cm^{-2} s^{-1})	$L_* (d/140\,\mathrm{pc})^2$ ($L_\odot$)
V807 Tau A	K7	4060	0.03 ± 0.42	0.14 ± 0.03	1.72 ± 0.32	1.05 ± 0.20
V807 Tau Ba	M2	3560	0.61 ± 0.50	0.12 ± 0.01	0.732 ± 0.094	0.447 ± 0.058
V807 Tau Bb	M2−M2.5	3560	1.18 ± 0.47	0.11 ± 0.01	0.483 ± 0.063	0.356 ± 0.038

Notes. The uncertainty in the distance (±10 pc) contributes an additional systematic uncertainty of ± 0.16, 0.066, and 0.053 $L_\odot$ to the luminosities of A, Ba, and Bb, respectively.

a filter at wavelength λ. We then fit low-resolution spectral models computed by Kurucz and Castelli[9,10] to the measured photometry. We averaged the flux of the stellar models across the width of each of the observed filter bands. The emergent flux from the star given by the models scales as the area subtended on the sky (or as the square of the stellar angular diameter). Therefore, fitting the SED with stellar models is dependent on three parameters, the effective temperature T_{eff} of the stellar model, the angular diameter of the star θ, and the interstellar extinction A_V in the V band. The SED fits also provide an estimate of the bolometric flux $F_{bol} = (1/4)\theta^2 \sigma T^4$ and the luminosity $L = 4\pi d^2 F_{bol}$.

We converted the spectral types determined from the NIRSPAO spectra to effective temperatures using the dwarf spectral type temperature relations used in Kraus & Hillenbrand (2007) for K0−M0 and the T Tauri temperature scale defined in Luhman et al. (2003) for M1−M7. We fixed these temperatures when computing the SED fits and determined uncertainties by varying the model spectrum by one spectral step (∼250 K) and calculating the range of variation in the derived parameters. We know from the FGS photometry that V807 Tau A is variable (see Figure 15 in Schaefer et al. 2006); this is consistent with its classification as a classical T Tauri star. To account for the variability potentially being propagated through to the magnitudes of the individual components, we applied a floor uncertainty of 0.1 mag to all of the magnitudes listed Table 4. In Table 9, we list the spectral type, adopted T_{eff}, and the parameters derived from the SED fit including A_V, θ, F_{bol}, and L. Figure 9 shows plots of the SED fits. For V807 Tau A, we did not include the K- and L-band magnitudes in the fit because they are affected by the infrared excess from the circumstellar disk. Therefore, the luminosity we calculate for V807 Tau A should mostly reflect the star, with little contamination from the disk. The SED fits for V807 Tau Ba and Bb show that the infrared magnitudes are well matched by the spectral templates, confirming that there is no evidence for circumstellar disks around these weak-lined T Tauri stars (White & Ghez 2001; Hartigan & Kenyon 2003). The luminosities we derive are in agreement with the estimates for the A−B components determined by White & Ghez (2001). The presence of a disk can also be identified by a dereddened $K − L$ color in excess of 0.4 (e.g., Prato et al. 2003). Converting the Two Micron All Sky Survey (2MASS) K_s magnitudes to the Bessell–Brett homogenized system (Carpenter 2001) and averaging the two K-band magnitudes from Table 4, we obtain dereddened $K − L = 0.86 ± 0.14$ mag for V807 Tau A and $0.31 ± 0.27$ mag and $0.05 ± 0.35$ mag for Ba and Bb, respectively. As with the SED fits, these values show strong evidence

for a disk in V807 Tau A and the absence of a disk around Ba and Bb.

3.3. Comparison of Radio and Infrared Positions

We detected a compact radio source in three of the six epochs of VLBA observations. Using the optical coordinates and proper motion of V807 Tau in Ducourant et al. (2005), we computed the location of the optical source during the times of the VLBA epochs. Assuming that the optical coordinates are dominated by the light from V807 Tau A and using the relative positions of V807 Tau A, Ba, and Bb from the AO images, we find that the VLBA coordinates are consistent with the location of the close pair to within ∼50 mas. The standard error on the optical coordinates is ∼39 mas (Ducourant et al. 2005).

To determine whether the radio emission is coming from V807 Tau Ba or Bb, we used our astrometric orbital fit (Figure 7) to compute the predicted locations of Ba and Bb during the times of the VLBA observations. We then applied the appropriate parallactic shift caused by a parallax of 7.14 mas (using the 140 pc distance from Kenyon et al. 1994) and added in the proper motion to compare the infrared positions with the motion observed in the VLBA reference frame. During the two epochs with a detection of only a single source, we find that the radio position is consistent with the infrared location of V807 Tau Ba on 2007 March 10 and 2008 August 28. On 2008 March 19, the faint radio source agrees with the infrared location of V807 Tau Ba while the brighter radio source matches the location of V807 Tau Bb. The relative position of the two radio sources during this epoch ($\rho = 37.75$ mas, P.A. = 75°04) agrees quite nicely with the predicted position based on our orbit fit ($\rho = 37.80$ mas, P.A. = 75°00).

To minimize the difference between the infrared and radio positions, we adjusted the parallax, proper motion, and the relative shift between the two frames. Following this approach, we determined a best-fitting parallax of $\pi = 7.3 ± 1.2$ mas and proper motion of $\mu_\alpha \cos \delta = 7.6 ± 1.8$ mas yr^{-1}, $\mu_\delta = -13.0 ± 1.4$ mas yr^{-1}. We show a comparison of the radio and infrared positions using these proper motions in Figure 10. Our measurements are consistent with the range of proper motions measured for stars in the Taurus star-forming region (Ducourant et al. 2005; Bertout & Genova 2006). They are marginally consistent with the proper motion measured individually for V807 Tau by Ducourant et al. (2005) ($\mu_\alpha \cos \delta = 10$ mas yr^{-1}, $\mu_\delta = -20$ mas yr^{-1}). The optical measurement could be affected by an offset in the photocenter caused by the orbital motion of the three components in the system which might account for the discrepancy in μ_δ. We note that V807 Tau lies within the same region of the Taurus cloud complex as HP Tau/G2, a target that has a reliable parallax and proper motion measured using the VLBA (see spatial distribution of VLBA sources in Figure 5 of Torres et al. 2009). The
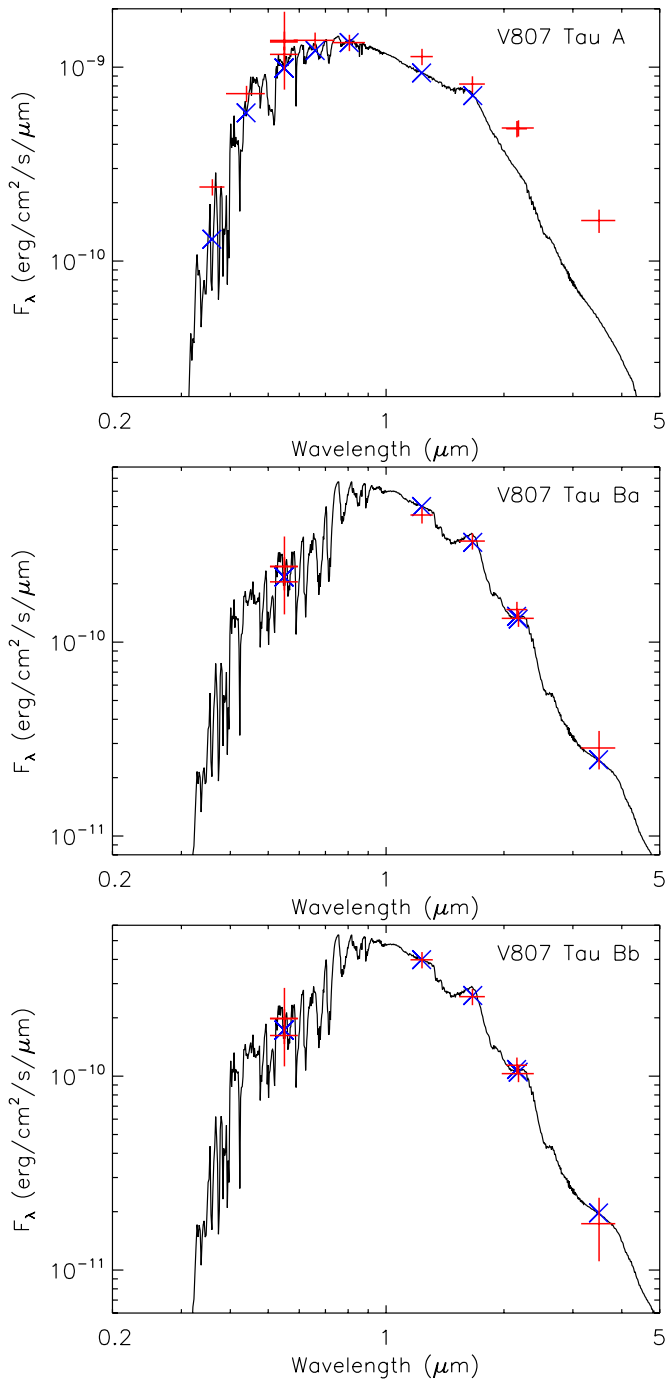
---

9 http://kurucz.harvard.edu/grids.html
10 http://wwwuser.oat.ts.astro.it/castelli/grids/gridp00k0odfnew/fp00k0tab.html

Figure 9. Spectral energy distributions for V807 Tau A (top), V807 Tau Ba (middle), and V807 Tau Bb (bottom). The best-fitting Kurucz model is represented by the solid black line. The average model flux across the given photometric band is shown by the blue crosses. The red plus symbols show the measured photometric magnitudes; the vertical length gives the size of the measurement error in the magnitudes while the horizontal width represents the width of the photometric filter.

(A color version of this figure is available in the online journal.)

Figure 10. Relative positions measured for the radio source during the three VLBA epochs (asterisks). For reference, we overplot the infrared positions of V807 Tau Ba and Bb determined from the astrometric orbit during these epochs (circles and squares, respectively). We applied our derived parallax of 7.3 ± 1.2 mas and proper motion of $\mu_\alpha \cos \delta = 7.3 \pm 1.2$ mas yr^{-1}, $\mu_\delta = -13.0 \pm 1.4$ mas yr^{-1} to the infrared positions. The arrow indicates the direction and magnitude of the proper motion over the course of a year.

proper motion we measure for V807 Tau is similar to that measured for HP Tau/G2 ($\mu_\alpha \cos \delta = 13.85 \pm 0.03$ mas yr^{-1}, $\mu_\delta = -15.4 \pm 0.02$ mas yr^{-1}, $\pi = 6.20 \pm 0.03$ mas), as would be expected from two sources that might be located physically near to each other.

Ultimately, our goal is to combine these multi-epoch VLBA observations of V807 Tau to derive a distance with 2%–4% precision, similar to that obtained for other young stars in

Taurus and Ophiuchus (Lestrade et al. 1999; Loinard et al. 2005, 2008; Torres et al. 2007, 2009, 2012). Our preliminary parallax has a much larger uncertainty, but is consistent with the range of distances measured for other members of the Taurus star-forming region (130–160 pc). It was difficult to obtain a more precise parallax for V807 Tau based on the current set of VLBA data because the radio emission from the two components is weak and variable and was not detected in half of the epochs. We plan to continue these observations in the future to improve the precision of our results.

Based on the VLBA maps, the size of the radio-emitting regions during each epoch is smaller than 2 mas ($\lesssim 60\ R_\odot$ or $\lesssim 40\ R_*$ assuming a stellar radius of 1.5 $R_\odot$). The lack of disk signatures associated with V807 Tau Ba and Bb suggests that the variable and compact radio emission likely arises from magnetic activity and reconnection flares in the stellar magnetospheres of each component (e.g., Feigelson & Montmerle 1999). The properties of the radio emission from V807 Tau Ba and Bb are consistent with those found around other weak-lined T Tauri stars which often show variability and the presence of radio flares (e.g., O'Neal et al. 1990; Feigelson et al. 1994). The compact size and correspondingly high brightness temperatures of radio emission associated with weak-lined T Tauri stars generally indicate a non-thermal emission source (Phillips et al. 1991; André et al. 1992). Using the major axis of the Gaussian models that we fit to the VLBA data as an upper limit to the size of the radio-emitting regions around V807 Tau Ba and Bb, we compute a brightness temperature ranging from 5.3×10^6 to 1.3×10^8 (using Equation (1) in Skinner 1993); this is consistent with the brightness temperatures expected from non-thermal emission ($\gtrsim 10^7$; André et al. 1992). Circular polarization is often undetected in radio-emitting weak-lined T Tauri stars, but has been detected occasionally in a few of the stronger sources, typically at a level of a few percent (e.g., White et al. 1992). The presence of circular polarization in the stronger sources indicates that the emission is likely gyrosynchrotron radiation. The upper limit on the degree of polarization measured
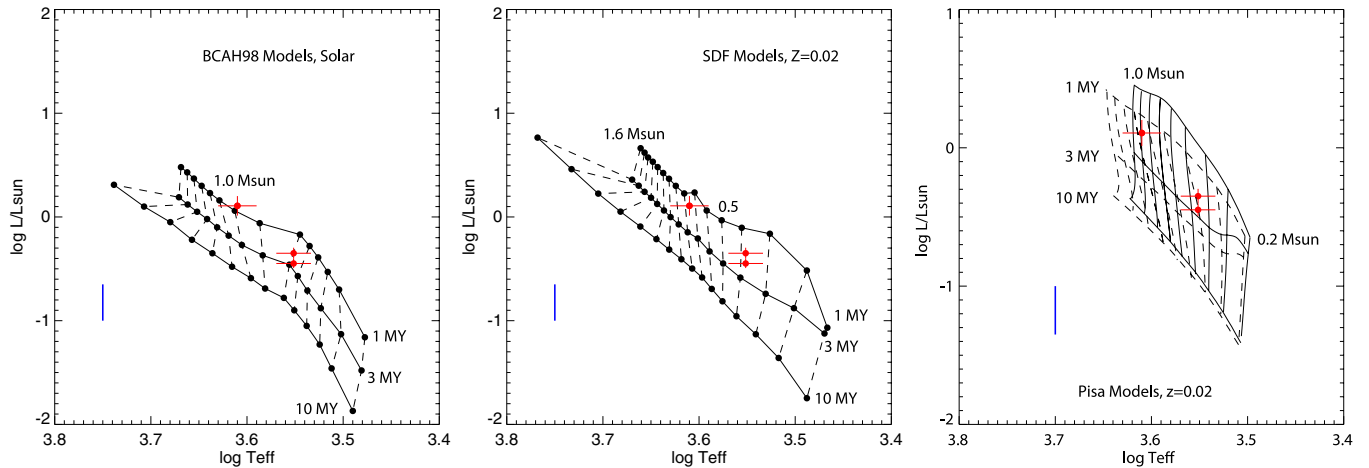
Figure 11. H-R diagrams showing the location of V807 Tau A, Ba, and Bb with respect to pre-main-sequence evolutionary tracks. Left: evolutionary tracks of Baraffe et al. (1998, BCAH98) at solar metallicity for masses of 0.1–1.4 $M_\odot$. For masses below 0.7 $M_\odot$, we used the tracks calculated with a mixing length parameter of 1.0; for larger masses we used the tracks with a mixing length of 1.9. Middle: evolutionary tracks of Siess et al. (2000, SDF) at $Z = 0.02$ for masses of 0.1–1.6 $M_\odot$. Right: Pisa stellar evolutionary models (Tognelli et al. 2011) for mixing length parameter of $\alpha = 1.20$ (solid lines) and $\alpha = 1.68$ (dashed lines) at a metallicity of $Z = 0.02$. The evolutionary tracks are plotted from 0.2 to 1.0 $M_\odot$ at 0.1 $M_\odot$ intervals. In all of the panels, the isochrones are plotted at 1, 3, and 10 Myr. The vertical blue bar represents the range of distances for stars located in the Taurus star-forming region, 140 ± 20 pc.

(A color version of this figure is available in the online journal.)

for V807 Tau ($<8\%$) is consistent with these expectations. In another young triple system, the close binary V773 Tau Aa$-$Ab ($P \sim 51$ days, $a \sim 0.3$–0.5 AU) shows enhanced radio flares during periastron passage (Massi et al. 2006, 2008; Torres et al. 2012). However, the larger separation between the components in V807 Tau Ba$-$Bb ($\sim$3.8–7.0 AU) makes it unlikely that similar inter-binary magnetic interactions would take place in the system.

4. DISCUSSION

4.1. Comparison with Evolutionary Tracks

We compare the locations of V807 Tau A, Ba, and Bb in the H-R diagram to theoretical models of PMS stellar evolution in Figure 11. We plot the luminosity and effective temperature of each component listed in Table 9 and compute expected masses and ages based on the evolutionary tracks computed by Baraffe et al. (1998, BCAH), Siess et al. (2000, SDF), and Tognelli et al. (2011, Pisa models).

The BCAH tracks predict a mass of $0.58 \pm 0.13\,M_\odot$ at an age of 2.5 ± 0.5 Myr for V807 Tau Ba and Bb and a mass of $0.76 \pm 0.15\,M_\odot$ at an age of 0.9 ± 0.2 Myr for V807 Tau A. The SDF tracks predict a mass of $0.38 \pm 0.08\,M_\odot$ at an age of 2.5 ± 0.5 Myr for V807 Tau Ba and Bb and a mass of $0.76 \pm 0.15\,M_\odot$ at an age of 2.0 ± 1.0 Myr for V807 Tau A. For the Ba and Bb components, the BCAH tracks predict a mass greater than the SDF tracks while the age estimates are about the same. Compared with the dynamical mass measurements at a distance of 140 pc, the BCAH tracks are in good agreement with the mass of Ba ($M_{\rm Ba} = 0.564\,(d/140\,{\rm pc})^3\,M_\odot$), while the SDF tracks underestimate its value by 2σ. For the Bb component ($M_{\rm Bb} = 0.476\,(d/140\,{\rm pc})^3\,M_\odot$), the BCAH tracks overestimate the dynamical mass while the SDF tracks underestimate the value, both by $\sim$1σ. The precision in determining the effective temperature based on our library of spectral templates limits our ability to discern finer differences in the predicted masses of V807 Tau Ba and Bb from the evolutionary tracks. Furthermore, if we include the uncertainty in the distance to V807 Tau, then each of the predicted evolutionary masses becomes consistent with the dynamical estimates to within 1σ. The uncertainty

in the distance can be improved independently, for example, by measuring a geometric parallax using the VLBA. The internal precision of the dynamical masses from the orbit fitting indicates that with an improved estimate of the distance, we can begin to make more meaningful comparisons between the evolutionary tracks.

For the Pisa models, we compare our results with tracks at solar metallicity ($Z = 0.02$, $Y = 0.288$, deuterium fraction 2×10^{-4}) using a mixing length parameter of $\alpha = 1.2$ and 1.68. For $\alpha = 1.2$, the Pisa tracks predict a mass of $0.46 \pm 0.10\,M_\odot$ at an age of 2.0 ± 1.0 Myr for V807 Tau Ba and Bb and a mass of $0.88 \pm 0.18\,M_\odot$ at an age of 2.0 ± 1.0 Myr for V807 Tau A. For the larger mixing length of $\alpha = 1.68$, the Pisa tracks predict a mass of $0.40 \pm 0.09\,M_\odot$ at an age of 2.5 ± 0.5 Myr for V807 Tau Ba and Bb and a mass of $0.68 \pm 0.18\,M_\odot$ at an age of 1.8 ± 0.5 Myr for V807 Tau A. Based on these results, it appears that the tracks at $\alpha = 1.2$ are more consistent with the dynamical masses of V807 Tau Ba and Bb at a distance of 140 pc. As mentioned previously, including the current uncertainty in the distance to V807 Tau makes this distinction less significant.

For the evolutionary models that we considered, the ages for the components of V807 Tau are approximately 2 Myr. This is in agreement with the mean age of 2.5 Myr determined from a larger census of the Taurus star-forming region in White & Ghez (2001). If all three components in V807 Tau formed at the same time, the agreement among the ages predicted for each component is more consistent for the SDF and Pisa tracks than it is for the BCAH models. The age of the system depends on the actual distance to V807 Tau. Because the distance provides the same scaling factor for all three components, the relative coevality between the components should remain consistent for a given set of tracks while the absolute age will shift. For members of the Taurus star-forming region with accurate VLBA parallaxes, the spread in distance ranges from 130 to 160 pc (Torres et al. 2009). Our comparisons assume a distance of 140 pc. If the distance proves to be closer to 160 pc (as the location of V807 Tau in Figure 5 of Torres et al. 2009 might suggest), then the luminosities will be 0.12 dex greater and the ages would turn out to be closer to 1 Myr.

4.2. Component Rotation

Assuming that the rotational axes of V807 Tau A, Ba, Bb, and the orbital axis of the Ba−Bb binary are aligned, the projected rotational velocities we measured imply that Ba and Bb ($v \sin i$ = 60–70 km s^{-1}) are rotating much faster than A ($v \sin i$ = 15 km s^{-1}). As discussed in Section 3.2, V807 Tau A is identified as a classical T Tauri star with an infrared excess from a circumstellar disk, while V807 Tau Ba and Bb are classified as weak-lined T Tauri stars without any evidence for a disk. The most efficient method for young stars to shed angular momentum is through disk locking (e.g., Stassun & Terndrup 2003; Dahm et al. 2012). Therefore, the presence of a disk around V807 Tau A and none within the V807 Tau B pair may explain the large difference in the rotational velocities between the components. The difference in rotational velocities in the V807 Tau system is also consistent with the study by Meibom et al. (2007) which shows that young, close binaries typically rotate faster than single stars and wider binaries, as a consequence of the close companion shortening the lifetime of the circumstellar disk and, in turn, the amount of time available for disk-braking.

The break-up velocity of a 0.5 $M_\odot$ star is ∼203 km s^{-1} using a radius of ∼1.5 $R_\odot$ at 2 Myr (Siess et al. 2000). If the rotational axes of Ba and Bb are inclined by about the same amount as the orbital inclination of the Ba−Bb binary, $i \sim 152°$, then they are actually rotating about twice as fast, $v \sim 140$ km s^{-1}, or about two-thirds of breakup. The rotational velocity measured for V807 Tau Ba and Bb is higher than the average value of $v \sin i \sim 11$ km s^{-1} measured for M-stars in the Taurus star-forming region (Nguyen et al. 2009); however there are individual low-mass young stars which have projected rotational velocities similar to V807 Tau Ba and Bb. To remove the dependence on the inclination from this comparison, we can convert the estimated rotational velocity of the components in V807 Tau Ba and Bb to a rotation period of ∼0.5 days (using $R_* \sim 1.5 R_\odot$) and compare to the rotation periods measured for stars in young clusters. As shown in Irwin & Bouvier (2009), although it is rare for low-mass young stars to be rotating so rapidly, there are other ∼0.5 $M_\odot$ stars present in nearby young clusters that have similarly short rotation periods at an age of about 2–5 Myr.

5. SUMMARY

1. We measured the orbital motion within the PMS triple, V807 Tau, using AO imaging at the Keck Observatory. The relative orbit of V807 Tau Ba−Bb combined with the motion of Ba and Bb around their center of mass, measured relative to V807 Tau A, yields dynamical masses of $M_{Ba} = 0.564 \pm 0.018 \ (d/140 \, pc)^3 \ M_\odot$ and $M_{Bb} = 0.476 \pm 0.017 \ (d/140 \, pc)^3 \ M_\odot$. The uncertainty in the masses represent the errors computed from the orbit fit; the systematic uncertainty in the distance is reflected by the additional scaling factor.

2. Based on spatially resolved high-resolution spectra, we determined the spectral types of K7 for V807 Tau A and M2 for V807 Tau Ba and Bb. The broadening of the spectral lines indicates that V807 Tau A is rotating with a projected velocity of 15 km s^{-1}. The spectra of V807 Tau Ba and Bb are rotationally broadened by 65–70 km s^{-1}. If the rotational axes of the three stars are aligned, this indicates that the components in the close pair are rotating much more quickly than V807 Tau A.

3. The SED of V807 Tau A shows an excess above the stellar model in the K and L bands. This is consistent with its classification as a classical T Tauri star with an accretion disk. The SEDs for V807 Tau Ba and Bb show that the infrared magnitudes are well matched by the spectral templates, consistent with a lack of circumstellar material around these weak-lined T Tauri stars.

4. Uncertainties in the distance to the system and the effective temperatures of the components are the main limitations to a more detailed comparison of our dynamical mass measurements with predictions based on evolutionary tracks for PMS stars. At a distance of 140 pc, the tracks indicate an age of ∼2 Myr for the V807 Tau triple.

5. We detected compact radio emission from V807 Tau during three out of six epochs using the VLBA. The emission is variable, with the integrated intensity ranging from 0.52 to 8.60 mJy. Comparing the position of the radio source with the motion observed in our infrared images, we determined that the emission originated from V807 Tau Ba in the first and third detected epochs, while both V807 Tau Ba and Bb were detected in the second epoch. Continued monitoring with the VLBA in the future will provide a precise parallax measurement for V807 Tau. This will help place the dynamical masses on an absolute scale.

Facilities: Keck:II (NIRC2, NIRSPEC), VLBA

REFERENCES

Andersen, J. 1991, A&AR, 3, 91
André, P., Deeney, B. D., Phillips, R. B., & Lestrade, J.-F. 1992, ApJ, 401, 667

Baraffe, I., Chabrier, G., Allard, F., & Hauschildt, P. H. 1998, A&A, 337, 403
Bender, C., Simon, M., Prato, L., Mazeh, T., & Zucker, S. 2005, AJ, 129, 402
Bertout, C., & Genova, F. 2006, A&A, 460, 499
Blake, C. H., Charbonneau, D., White, R. J., Marley, M. S., & Saumon, D. 2007, ApJ, 666, 1198
Boden, A. F., Sargent, A. I., Akeson, R. L., et al. 2005, ApJ, 635, 442
Boden, A. F., Torres, G., Sargent, A. I., et al. 2007, ApJ, 670, 1214
Cardelli, J. A., Clayton, G. C., & Mathis, J. S. 1989, ApJ, 345, 245
Carpenter, J. M. 2001, AJ, 121, 2851
Cotton, W. D. 1993, AJ, 106, 1241
Cutri, R. M., Skrutskie, M. F., van Dyk, S., et al. 2003, 2MASS All Sky Catalog of Point Sources (Pasadena, CA: NASA/IPAC)
Dahm, S. E., Slesnick, C. L., & White, R. J. 2012, ApJ, 745, 56
Duchêne, G., Beust, H., Adjali, F., Konopacky, Q. M., & Ghez, A. M. 2006, A&A, 457, L9
Ducourant, C., Teixeira, R., Périé, J. P., et al. 2005, A&A, 438, 769
Feigelson, E. D., & Montmerle, T. 1999, ARA&A, 37, 363
Feigelson, E. D., Welty, A. D., Imhoff, C., et al. 1994, ApJ, 432, 373
Fomalont, E., & Kogan, L. 2005, ATMCA: Phase Referencing Using More than One Calibrator (AIPS Memo 111; Socorro, NM: NRAO)
Ghez, A. M., Neugebauer, G., & Matthews, K. 1993, AJ, 106, 2005
Ghez, A. M., Weinberger, A. J., Neugebauer, G., Matthews, K., & McCarthy, D. W., Jr. 1995, AJ, 110, 753
Hartigan, P., & Kenyon, S. J. 2003, ApJ, 583, 334
Hartkopf, W. I., McAlister, H. A., & Franz, O. G. 1989, AJ, 98, 1014
Holfeltz, S. T., Nelan, E. P., Taff, L. G., & Lattanzi, M. G. 1995, *Hubble Space Telescope* Fine Guidance Sensor Instrument Handbook, Version 5.0 (Baltimore, MD: STScI)
Irwin, J., & Bouvier, J. 2009, in IAU Symp. 258, The Ages of Stars, ed. E. E. Mamajek, D. R. Soderblom, & R. F. G. Wyse (Cambridge: Cambridge Univ. Press), 363
Kenyon, S. J., Dobrzycka, D., & Hartmann, L. 1994, AJ, 108, 1872
Kharchenko, N. V. 2001, Kinematika Fiz. Nebesnykh Tel, 17, 409
Kharchenko, N. V., & Roeser, S. 2009, VizieR Online Data Catalog, 1280, 0
Kraus, A. L., & Hillenbrand, L. A. 2007, AJ, 134, 2340
Leinert, C., Zinnecker, H., Weitzel, N., et al. 1993, A&A, 278, 129
Leppänen, K. J., Zensus, J. A., & Diamond, P. J. 1995, AJ, 110, 2479
Lestrade, J.-F., Preston, R. A., Jones, D. L., et al. 1999, A&A, 344, 1014
Lister, M. L., Cohen, M. H., Homan, D. C., et al. 2009, AJ, 138, 1874
Loinard, L., Mioduszewski, A. J., Rodríguez, L. F., et al. 2005, ApJ, 619, L179
Loinard, L., Torres, R. M., Mioduszewski, A. J., & Rodríguez, L. F. 2008, ApJ, 675, L29
Luhman, K. L., Stauffer, J. R., Muench, A. A., et al. 2003, ApJ, 593, 1093
Massi, M., Forbrich, J., Menten, K. M., et al. 2006, A&A, 453, 959
Massi, M., Ros, E., Menten, K. M., et al. 2008, A&A, 480, 489
Mazeh, T., Prato, L., Simon, M., et al. 2002, ApJ, 564, 1007
McLean, I. S., Becklin, E. E., Bendiksen, O., et al. 1998, Proc. SPIE, 3354, 566
McLean, I. S., Graham, J. R., Becklin, E. E., et al. 2000, Proc. SPIE, 4008, 1048

Meibom, S., Mathieu, R. D., & Stassun, K. G. 2007, ApJ, 665, 155
Mioduszewski, A. J., & Kogan, L. 2009, Strategy for Removing Tropospheric and Clock Errors Using DELZN Version 2.0 (AIPS Memo 110; Socorro, NM: NRAO)
Napier, P. J. 1995, in ASP Conf. Ser. 82, Very Long Baseline Interferometry and the VLBA, ed. J. A. Zensus, P. J. Diamond, & P. J. Napier (San Francisco, CA: ASP), 59
Napier, P. J., Bagri, D. S., Clark, B. G., et al. 1994, IEEE Proc., 82, 658
Nguyen, D. C., Jayawardhana, R., van Kerkwijk, M. H., et al. 2009, ApJ, 695, 1648
O'Donnell, J. E. 1994, ApJ, 422, 158
O'Neal, D., Feigelson, E. D., Mathieu, R. D., & Myers, P. C. 1990, AJ, 100, 1610
Phillips, R. B., Lonsdale, C. J., & Feigelson, E. D. 1991, ApJ, 382, 261
Prato, L., Greene, T. P., & Simon, M. 2003, ApJ, 584, 853
Prato, L., Simon, M., Mazeh, T., et al. 2002, ApJ, 569, 863
Prato, L. A. 1998, PhD thesis, State Univ. New York at Stony Brook
Rosero, V., Prato, L., Wasserman, L. H., & Rodgers, B. 2011, AJ, 141, 13
Rousselot, P., Lidman, C., Cuby, J.-G., Moreels, G., & Monnet, G. 2000, A&A, 354, 1134
Schaefer, G. H., Simon, M., Beck, T. L., Nelan, E., & Prato, L. 2006, AJ, 132, 2618
Schaefer, G. H., Simon, M., Nelan, E., & Holfeltz, S. T. 2003, AJ, 126, 1971
Schaefer, G. H., Simon, M., Prato, L., & Barman, T. 2008, AJ, 135, 1659
Schlieder, J. E., Lépine, S., Rice, E., et al. 2012, AJ, 143, 114
Shepherd, M. C. 1997, in ASP Conf. Ser. 125, Astronomical Data Analysis Software and Systems VI, ed. G. Hunt & H. Payne (San Francisco, CA: ASP), 77
Siess, L., Dufour, E., & Forestini, M. 2000, A&A, 358, 593
Simon, M., Ghez, A. M., Leinert, Ch., et al. 1995, ApJ, 443, 625
Simon, M., Holfeltz, S. T., & Taff, L. G. 1996, ApJ, 469, 890
Simon, M., & Prato, L. 2004, ApJ, 613, 69
Skinner, S. L. 1993, ApJ, 408, 660
Stassun, K. G., & Terndrup, D. 2003, PASP, 115, 505
Steffen, A. T., Mathieu, R. D., Lattanzi, M. G., et al. 2001, AJ, 122, 997
Tognelli, E., Prada Moroni, P. G., & Degl'Innocenti, S. 2011, A&A, 533, 109
Torres, R. M., Loinard, L., Mioduszewski, A. J., & Rodríguez, L. F. 2007, ApJ, 671, 1813
Torres, R. M., Loinard, L., Mioduszewski, A. J., & Rodríguez, L. F. 2009, ApJ, 698, 242
Torres, R. M., Loinard, L., Mioduszewski, A. J., et al. 2012, ApJ, 747, 18
van Moorsel, G., Kemball, A., & Greisen, E. 1996, in ASP Conf. Ser. 101, Astronomical Data Analysis Software and Systems V, ed. G. H. Jacoby & J. Barnes (San Francisco, CA: ASP), 37
White, R. J., & Ghez, A. M. 2001, ApJ, 556, 265
White, S. M., Pallavicini, R., & Kundu, M. R. 1992, A&A, 259, 149
Wizinowich, P. L., Acton, D. S., Lai, O., et al. 2000, Proc. SPIE, 4007, 2
Yelda, S., Lu, J. R., Ghez, A. M., et al. 2010, ApJ, 725, 331